

# Analysis of the Structure and Function of FOX-4 Cephamycinase

S. T. Lefurgy,<sup>a</sup> V. N. Malashkevich,<sup>b</sup> J. T. Aguilar,<sup>b</sup> E. Nieves,<sup>b</sup> E. C. Mundorff,<sup>a</sup> B. Biju,<sup>a</sup> M. A. Noel,<sup>a</sup> R. Toro,<sup>b</sup> D. Baiwir,<sup>h</sup> K. M. Papp-Wallace,<sup>c,d</sup> S. C. Almo,<sup>b</sup> J.-M. Frere,<sup>i</sup> G. Bou,<sup>j</sup> R. A. Bonomo<sup>c,d,e,f,g</sup>

Department of Chemistry, Hofstra University, Hempstead, New York, USA<sup>a</sup>; Department of Biochemistry, Albert Einstein College of Medicine, Bronx, New York, USA<sup>b</sup>; Research Service, Louis Stokes Cleveland Veterans Affairs Medical Center, Cleveland, Ohio, USA<sup>c</sup>; Departments of Medicine,<sup>d</sup> Pharmacology,<sup>e</sup> Molecular Biology and Microbiology,<sup>f</sup> and Biochemistry,<sup>g</sup> Case Western Reserve University, Cleveland, Ohio, USA; GIGA Proteomic Facility, Mass Spectrometry Laboratory GIGA-R, Université de Liège, Sart-Tilman, Liège, Belgium<sup>h</sup>; Centre d'Ingénierie des Protéines, Institut de Chimie, Université de Liège, Sart-Tilman, Liège, Belgium<sup>i</sup>; Servicio de Microbiología, Complejo Hospitalario Universitario A. Coruña, La Coruña, Spain<sup>j</sup>

**Class C  $\beta$ -lactamases poorly hydrolyze cephamycins (e.g., cefoxitin, cefotetan, and moxalactam). In the past 2 decades, a new family of plasmid-based AmpC  $\beta$ -lactamases conferring resistance to cefoxitin, the FOX family, has grown to include nine unique members descended from the *Aeromonas caviae* chromosomal AmpC. To understand the basis for the unique cephamycinase activity in the FOX family, we determined the first X-ray crystal structures of FOX-4, apo enzyme and the acyl-enzyme with its namesake compound, cefoxitin, using the Y150F deacylation-deficient variant. Notably, recombinant expression of N-terminally tagged FOX-4 also yielded an inactive adenylylated enzyme form not previously observed in  $\beta$ -lactamases. The post-translational modification (PTM), which occurs on the active site Ser64, would not seem to provide a selective advantage, yet might present an opportunity for the design of novel antibacterial drugs. Substantial ligand-induced changes in the enzyme are seen in the acyl-enzyme complex, particularly the R2 loop and helix H10 (P289 to N297), with movement of F293 by 10.3 Å. Taken together, this study provides the first picture of this highly proficient class C cephamycinase, uncovers a novel PTM, and suggests a possible cephamycin resistance mechanism involving repositioning of the substrate due to the presence of S153P, N289P, and N346I substitutions in the ligand binding pocket.**

Upon their discovery in the early 1970s, cephamycins were regarded as a solution to the emerging problem of cephalosporin-resistant bacteria (1). Derived from a bacterial natural product, cephamycin C, the pharmacology of this class of compounds parallels that of the cephalosporins, so these compounds (including cefoxitin, moxalactam, and cefotetan) are sometimes categorized as “second-generation” cephalosporins (see Fig. 1) (2). They contain the characteristic 7- $\alpha$ -methoxy group, which was shown to be essential for their recalcitrance to  $\beta$ -lactamase hydrolysis. At its introduction, cefoxitin displayed clinical activity against Gram-negative, Gram-positive, and anaerobic bacteria (3). As a consequence, cephamycins became widely used drugs to treat and even prevent infections. Cefoxitin was first approved for use in the United States in 1977 and was the highest-selling hospital drug in 1984 (4). Cefoxitin's initial effectiveness led to a recognized pattern of clinical overuse that may have contributed to the development of resistant  $\beta$ -lactamases (5). In addition, reduced permeability contributed to cephamycin resistance in *Enterobacteriaceae* (6).

Resistance to cefoxitin seems to have emerged spontaneously many times in Ambler class C  $\beta$ -lactamases, as opposed to having occurred through a single event and subsequent spread (7). The spread of cephamycin resistance was accelerated by the appearance of plasmid-based  $\beta$ -lactamases (8). There are now >150 known  $\beta$ -lactamases that significantly hydrolyze cephamycins (9), the most widespread of which is the plasmid-based CMY-2 (10). The CMY family of cephamycinases has been characterized with respect to structure and function, and the origin of their resistance to cefoxitin has been linked to alterations in the R2 substrate-binding loop that encompasses helix H10 (11, 12). Insertions and deletions in this region that widen the binding pocket correlate with a gain in the ability to hydrolyze cephamycins and expanded-spectrum cephalosporins.

The FOX family of cephamycinases was first observed in 1994 (13). The family has grown to include 10 related variants (nine are unique, as FOX-5 and FOX-6 possess the same sequence). None of them have been structurally described until now. The FOX family is distantly related to other cephamycinases and is thus an important enzyme to compare with the CMY and MOX families, which have been structurally characterized (Protein Data Bank identifiers [PDB IDs] 1ZKJ, 1ZC2, and 3W8K). Importantly, the FOX cluster lacks the shortened R2 loop seen in CMY-10 and MOX-1 enzymes (Fig. 2).

The structural origin of cephamycinase activity in FOX enzymes is not well understood. Mallo et al. (14) established that the deletion of a tripeptide (Gly-286, Ser-287, and Asp-288) in the R2 loop demonstrated little effect on cefoxitin hydrolysis. Clearly, factors beyond the length of the R2 loop govern cefoxitin hydrolysis in this family. Substitution of the conserved N346 for isoleucine is often seen in extended-spectrum AmpCs and cephamycinases and is implicated in substrate specificity switching toward carbapenems (15). The development of carbapenemase activity among cephamycinases is a particular concern due to the structural similarity between the two classes of antibiotics.

The active-site motifs in FOX-4 are shared by all class C  $\beta$ -lac-

Received 3 August 2015 Returned for modification 2 September 2015

Accepted 14 October 2015

Accepted manuscript posted online 2 November 2015

**Citation** Lefurgy ST, Malashkevich VN, Aguilar JT, Nieves E, Mundorff EC, Biju B, Noel MA, Toro R, Baiwir D, Papp-Wallace KM, Almo SC, Frere J-M, Bou G, Bonomo RA. 2016. Analysis of the structure and function of FOX-4 cephamycinase. *Antimicrob Agents Chemother* 60:717–728. doi:10.1128/AAC.01887-15.

Address correspondence to R. A. Bonomo, robert.bonomo@va.gov.

Copyright © 2016, American Society for Microbiology. All Rights Reserved.

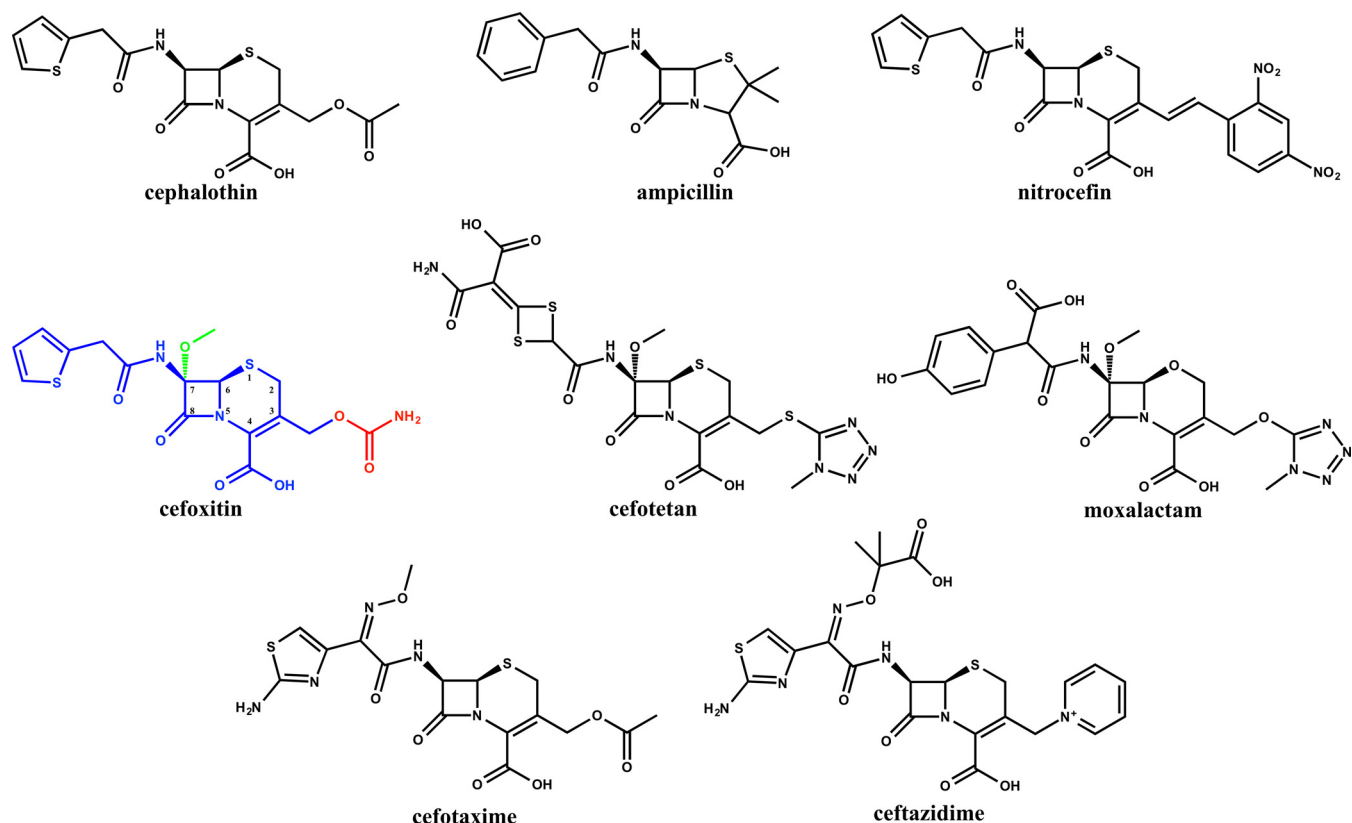


FIG 1 Compounds used in this study and other cephamycins. Cefoxitin is shown in blue, the 7- $\alpha$ -methoxyl group is shown in green, and the carboxamide side chain that is eliminated upon acylation of S64 is shown in red.

tamases: SXXX (positions 64 to 67), YXN (positions 150 to 152), and KTG (positions 315 to 317) (Fig. 2). For clarity, we will refer to the residues of FOX-4 by the canonical numbering of *Enterobacter cloacae* P99 AmpC (16). Compared to P99, the chain of FOX-4 is two residues shorter, due to a slightly longer signal peptide. There is a Ser residue inserted after the conserved Y203 in an exposed loop and a 2-residue deletion corresponding to P99 positions 242 and 243; both chain alterations occur on the protein surface, are distal to the active site, and are compensated by shifts in the chain that do not reveal any obvious structural differences in the substrate-binding region. The main differences in the substrate-binding region are the composition of the R2 loop and the residue at position Xaa346. Comparing known sequences of cephamycinases to noncephamycinases (e.g., chromosomal AmpC enzymes from *E. cloacae* P99, *Escherichia coli* K-12, and *Citrobacter freundii*), the sequence of FOX-4 aligns well in all regions except the R2 region. The side chain substitutions that result in cephamycinase activity are not readily evident by an examination of the primary sequence. Furthermore, the designations of cephamycinase and noncephamycinase enzymes, based on MIC results, are not clearly reflected in the steady-state kinetic constants. Often, the same catalytic efficiency is achieved by enzymes from each category (Table 2, compare the susceptible AmpC of *E. cloacae* P99 to the resistant AmpC of *Pseudomonas aeruginosa*). The  $k_{\text{cat}}$  values, however, seem to correlate with a resistance phenotype, except in the case of AmpC from *E. coli* K-12, for which there is an elevation in the  $K_m$  value. Therefore, the  $k_{\text{cat}}$  value may be a better measure of resistance toward cefoxitin.

To investigate the structural basis of cephamycin resistance in the FOX enzymes, the X-ray crystal structure of the family member FOX-4 was determined in the presence and absence of its namesake ligand, cefoxitin. This work first required the identification and ablation of a posttranslational modification (PTM) by adenylate (AMP) on S64. Steady-state kinetic constants were obtained for the unmodified enzyme with a few representative compounds (Fig. 1). The structural basis of cephamycinase activity is proposed.

## MATERIALS AND METHODS

**Reagents and compounds.** Lysogeny broth (LB) powder was purchased from Thermo Fisher Scientific (Springfield, NJ). Nitrocefin was purchased from TOKU-E (Bellingham, WA). Unless otherwise specified, all chemicals were from Sigma-Aldrich (St. Louis, MO) and were of the highest grade available.

**Site-directed mutagenesis.** The S64A and Y150F substitutions were generated in an expression plasmid carrying recombinant, tagged *bla*<sub>FOX-4</sub> using the QuikChange Lightning site-directed mutagenesis kit (Agilent Technologies, Santa Clara, CA). The primer pairs (Life Technologies, Carlsbad, CA) containing mutant codons (underlined) were S64Afor (CTGTTTCGAGATTGGCGCGGTACGAAGACCC), S64Arev (GGGTCTTGCTGACCGCGCCAATCTCGAACAG), Y150Ffor (GGACTCATCGCCAGTTTTCACACCCAGCAT), and Y150Frev (ATGCTGGGGTTGGA~~AA~~ACTGGCGATGAGTCC). The mutagenic PCRs were carried out on a MyCycler thermal cycler (Bio-Rad, Hercules, CA), according to the manufacturer's instructions.

**Protein expression and purification.** Recombinant FOX-4  $\beta$ -lactamase was produced from an expression vector (pHMTEV) that added a

FOX-4	---SGEAPLTATVDGIIQPM LKAYRIPGMAVAVLKDGAHYFNYGVANRESGQRVSEQTL	57
MOX-1	GEASPDVPLRPVVDASIQPLLKEHRIIPGMAVAVLKDGAHYFNYGVANRESGASVSEQTL	60
CMY-10	GEASPDVPLRPVVDASIQPLLKEHRIIPGMAVAVLKDGAHYFNYGVANRESGAGVSEQTL	60
ADC-7	DNTPKDQEIKKLVQDNFPLLEKYDVPGMAGVVIQNNKKYEMYYGLQSVQDKKAVNSSTI	60
AmpC <i>P. aeruginosa</i>	-GEAPADRLKALVDAAVQPMKANDIPGLAVAIISLKGEPHYFSYGLASKEDGRRVTPETL	59
CMY-2	-AAKTEQQIADIVNRTITPLMQEQAIIPGMAVAVIYQGKPYFTWGKADIANNHPVTQQT	59
AmpC <i>E. coli</i> K12	---APQQINDIVHRTITPLIEQQKIIPGMAVAVIYQGKPYFTWGYADIAKKQPVTPQTL	56
AmpC <i>C. freundii</i>	-AAKTEQQIADIVNRTITPLMQEQAIIPGMAVAVIYEGKPYFTWGKADIANNHPVTQQT	59
AmpC <i>E. cloacae</i> P99	-TPVSEKQLAEVVANTITPLMKAQSVPGMAVAVIYQGKPHYFTFGKADIAANKPVTPQTL	59
	: * . *:: : ***: . : : : * . * . *	
FOX-4	FEIGSVSKTLTATLGAYAAVKGGFELDDKVSQHAPWLKGSFAFDGVTMAELATYSAGGLPL	117
MOX-1	FEIGSVSKTLTATLGAYAVVKGAMQLDDKASRHAPWLKGSVFDSTITMGEATYSAGGLPL	120
CMY-10	FEIGSVSKTLTATLGAYAVVKGAMQLDDKASRHAPWLKGSFAFDSTITMGEATYSAGGLPL	120
ADC-7	FELGSVSKLTATAGGYAKNKGISFDDTPGKYWKELKNTPIDQVNLQLATYTSGLNAL	120
AmpC <i>P. aeruginosa</i>	FEIGSVSKTFTATLAGYALTQDKMRLDDRASQHPALQGSRFDDGISLLDLATYTAGGLPL	119
CMY-2	FELGSVSKTFNGVLGGDAIARGEIKLSDPVTKYWPELTGKQWQGIIRLLHLATYTAGGLPL	119
AmpC <i>C. freundii</i>	FELGSVSKTFNGVLGGDRIARGEIKLSDPVTKYWPELTGKQWRGISLLHLATYTAGGLPL	119
AmpC <i>E. coli</i> K12	FELGSVSKTFTGVLGGDAIARGEIKLSDPTTKYWPELTAKQWNGITLLHLATYTAGGLPL	116
AmpC <i>E. cloacae</i> P99	FELGSIKSTFTGVLGGDAIARGEISLDDAVTRYWPLTGKQWQGIIRMLDLATYTAGGLPL	119
	**::**::** :... : : : : * : : * : : : : **::**::**	
FOX-4	QFPDEVDSN-DKMQTYIRSWSVPYPAGTHROYSNPSIGLFGHLAANSLGQPFQELMSQTL	176
MOX-1	QFPDEVDSN-EKMRAYYRQWAPVYSPGSHRQYSNPSIGLFGHLAASSLKQPPAQLMEQTL	179
CMY-10	QFPDEVDSN-EKMRAYYRQWAPVYSPGSHRQYSNPSIGLFGHLAASSLKQPPAPLMEQTL	179
ADC-7	QFPDEVQTD-QQVLTFFKDWKPKNPIGEYRQYSNPSIGLFGKVVALLSMNKPFDQVLEKTI	179
AmpC <i>P. aeruginosa</i>	QFPDSVQKDAQIRDYRQWQPTYPAGSQRLYSNPSIGLFGYLAARSLGQPFERLMEQVQ	179
CMY-2	QIPDDVRDK-AALLHFYQNWQWPQWTPGAKRLYANSIGLFGALAVKPSGMSYEEAMTRRV	178
AmpC <i>C. freundii</i>	QIPGDVTDK-AELLRFYQNWQWPQWTPGAKRLYANSIGLFGALAVKSSGMSYEEAMTRRV	178
AmpC <i>E. coli</i> K12	QVPDEVKSS-SDLLRFYQNWQPAWAPGTQRLYANSIGLFGALAVKPSGLSFEQAMQTRV	175
AmpC <i>E. cloacae</i> P99	QVPDEVTDN-ASLLRFYQNWQWPQWKGTTRLYANSIGLFGALAVKPSGMPYEQAMTRV	178
	*. * . * : : : : * * * * * : : : : : *	
FOX-4	LPKLGHLHTYIQVPESAMANYAYGYSKEDKPIRATPGVLAEEAYGIKTSADLLKFVEAN	236
MOX-1	LPGLGMHHTYVNVPKQAMASYAYGYSKEDKPIRVNPGMLADEAYGIKTSADLLAFVKAN	239
CMY-10	LPGLGMHHTYVNVPKQAMASYAYGYSKEDKPIRVNPGMLADEAYGIKTSADLLRFVKAN	239
ADC-7	FEELGLKYSYVNVPKTQIQNYAFGYNQENQPIRVNPGPLDAPAYGVKSTLPDMLKFAN	239
AmpC <i>P. aeruginosa</i>	FPALGLEQTHLDVPEAALAQYAGQYKDDRLRVGPGPLDAEYGVKTSADLLRFVDAN	239
CMY-2	LQPLKLAHTWITVPQNEQKDYAWGY-REGKPVHVSPGQLDAEAYGVKSSVIDMARWQAN	237
AmpC <i>C. freundii</i>	LQPLKLAHTWITVPQSEQKNYAWGY-LEGKPVHVSPGQLDAEAYGVKSSVIDMARWQAN	237
AmpC <i>E. coli</i> K12	FQPLKLNHTWINVPAEEKNYAWGY-REGKAVHVSPGALDAEAYGVKSTIEDMARWQSN	234
AmpC <i>E. cloacae</i> P99	LKPLKLDHTWINVPAEEAHYAWGY-RDGKAVRVSPGMLDAQYGVKTNVQDMANWYMAN	237
	: * : : : ** ** * : : : . ** * . **::**::** : : : *	
FOX-4	MGYQ--GDAALKSAIALTHTGFSVGEMTQGLGWESYDYPVTEQVLLAGNSPAVSFQANP	294
MOX-1	IGGV--DDKALQQAISLTHKGHSYVGEMTQGLGWESYAYPVTEQTLLAGNSAKVILEANP	297
CMY-10	IGGV--DDKALQQAISLTHQGHSYVGEMTQGLGWESYAYPVTEQTLLAGNSAKVILEANP	297
ADC-7	LNPQK-YPADIQRAINETHQGFYQVNTMYQALGWEEFSYPATLQTLDDSNSEQIVMKPNK	298
AmpC <i>P. aeruginosa</i>	LHPER-LDRPWAQALDATHRGYKVGDMTQGLGWEAYDWPISLKRLQAGNSTPMALQPHR	298
CMY-2	MDASHVQEKTLQGGIALAQSRWRIGDMYQGLGWEMLNWLKADSIINGSDSKVALAALP	297
AmpC <i>C. freundii</i>	MDASHVQEKTLQGGIELAQSRWRIGDMYQGLGWEMLNWLKADSIINGSDSKVALAALP	297
AmpC <i>E. coli</i> K12	LKPLDINEKTLQGGIQLAQSRYWQTGDMYQGLGWEMLDWPVNPDSIINGSDNKIALAARP	294
AmpC <i>E. cloacae</i> P99	MAPENVADASLKQGGIALAQSRWRIGSMYQGLGWEMLNWPVEANTVVEGSDSKVALAPLP	297
	: : : : : * . **::**::** : * . : : . : : *	
FOX-4	VTRFAVPKAMGEQRLYNKTGSTGGFGAYVAFVPARGIAIVMLANRNPTEARVKAHAAIL	354
MOX-1	T---AAPRESGQSQVLFNKTGSTNGFGAYVAFVPARGIGIVMLANRNPTEARVKAHAAIL	354
CMY-10	T---AAPRESGQSQVLFNKTGSTNGFGAYVAFVPARGIGIVMLANRNPTEARIKAAHAIL	354
ADC-7	VTAS---KEPSVKMYHKTGSTNGFGTYVVFIPKENIGLVMLTNKRIPTEERIKAAAYAVL	355
AmpC <i>P. aeruginosa</i>	IARLPAPQALEGQRLNKTGSTNGFGAYVAFVPGRDGLVILANRNPTEARVKAHAAIL	358
CMY-2	AVEVNPPAPAVKASVWHKTGSTGGFGSYVAFVPEKNLGIIVMLANKSYNPVVEAAWRIL	357
AmpC <i>C. freundii</i>	AVEVNPPAPAVKASVWHKTGSTGGFGSYVAFVPEKNLGIIVMLANKSYNPVVEAAWRIL	357
AmpC <i>E. coli</i> K12	VKAITPPTPAVRASVWHKTGSTGGFGSYVAFIPEKELGIIVMLANKNYPNPARVDAWQIL	354
AmpC <i>E. cloacae</i> P99	VAEVNPPAPPVKASVWHKTGSTGGFGSYVAFIPEKQIGIVMLANTSYNPVVEAAAYHIL	357
	. **::**::** : **::**::** . : : : : * * . * . *	
FOX-4	SQLAE----- 359	
MOX-1	AQLAG----- 359	
CMY-10	AQLAG----- 359	
ADC-7	NAIKK----- 360	
AmpC <i>P. aeruginosa</i>	SGLEQQGKGVPLKR 371	
CMY-2	EKLQ----- 361	
AmpC <i>C. freundii</i>	EKLQ----- 361	
AmpC <i>E. coli</i> K12	NALQ----- 358	
AmpC <i>E. cloacae</i> P99	EALQ----- 361	
	:	

FIG 2 Multiple-sequence alignment of mature-length class C  $\beta$ -lactamases. Alignment was carried out using Clustal Omega. Conserved active-site motifs are shaded blue. The R2 loop is shaded yellow. Sequence motifs at positions 153 and 346 are shaded by residue type in magenta or green.

TABLE 1 Data collection and refinement statistics for the FOX-4 crystal structures

Parameter	Crystal structure		
	WT	Y150F	Y150F
Ligand			SFX
PDB entry	5CGS	5CGW	5CGX
Data collection			
Resolution range (Å)	20.0–1.6	20.0–1.4	20.0–1.2
Wavelength (Å)	0.979	0.979	0.979
Space group	P2 <sub>1</sub>	P2 <sub>1</sub>	P2 <sub>1</sub>
Unit cell dimensions (Å)			
a	54.85	53.22	54.24
b	57.09	56.61	56.59
c	56.75	54.18	55.49
$\alpha = \gamma$ (°)	90	90	90
$\beta$ (°)	96.45	96.24	99.23
No. of observed reflections	137,328	219,916	355,116
No. of unique reflections	41,748	62,564	96,864
Completeness (%) <sup>a</sup>	96.5 (87.1)	98.5 (93.8)	95.4 (92.2)
$I/\sigma I$	7.6 (2.1)	10.2 (2.5)	6.4 (1.6)
$R_{\text{merge}}$ ( $I$ ) <sup>b</sup>	0.080 (0.372)	0.073 (0.496)	0.070 (0.739)
Structural refinement			
$R_{\text{cryst}}$ (%) <sup>c</sup>	0.201	0.172	0.181
$R_{\text{free}}$ (%) <sup>c</sup>	0.230	0.207	0.205
No. of protein nonhydrogen atoms	2,704	2,781	2,797
No. of water molecules	220	443	379
Average B-factor (Å <sup>2</sup> )	17.2	14.0	11.4
RMSD from ideal value <sup>d</sup>			
Bonds (Å)	0.011	0.009	0.012
Angles (°)	1.36	1.33	1.43
Torsion angles (°)	14.1	12.6	14.3
Overall coordinate error (maximum-likelihood)	0.21	0.15	0.16
Ramachandran statistics (for non-Gly/Pro residues) (%)			
Most favorable	97.5	97.3	97.3
Additional allowed	2.5	2.7	2.7

<sup>a</sup> Values in parentheses indicate statistics for the high-resolution bin.

<sup>b</sup>  $R_{\text{merge}} = \sum_j |I_j(\text{hkl}) - \langle I(\text{hkl}) \rangle| / \sum_j I_j(\text{hkl})$ , where  $I_j$  is the intensity measurement for reflection  $j$ , and  $\langle I \rangle$  is the mean intensity over  $j$  reflections.

<sup>c</sup>  $R_{\text{cryst}}/(R_{\text{free}}) = \sum_j |F_o(\text{hkl}) - |F_c(\text{hkl})|| / \sum_j |F_o(\text{hkl})|$ , where  $F_o$  and  $F_c$  are the observed and calculated structure factors, respectively. No  $\sigma$ -cutoff was applied. Five percent of the reflections were excluded from refinement and used to calculate  $R_{\text{free}}$ .

<sup>d</sup> RMSD, root mean square deviation.

His<sub>9</sub>-maltose binding protein affinity tag and a spacer region containing the tobacco etch virus (TEV) protease recognition sequence to the N terminus of the mature-length FOX-4 (lacking the periplasmic signal sequence). Protein expression in *E. coli* BL21(DE3) was induced with 1 mM isopropyl  $\beta$ -D-1-thiogalactopyranoside (IPTG) for 20 h at 17°C. The cells were harvested by centrifugation and incubated at 4°C for 50 min with 0.1 mg/ml lysozyme, 200  $\mu$ M phenylmethylsulfonyl fluoride (PMSF), and 1 mM EDTA in 50 mM sodium phosphate buffer (pH 8.0). The cells were lysed by sonication and centrifuged at 17,500 rpm and 4°C for 50 min. The clarified lysate was diluted in loading buffer (50 mM sodium phosphate and 300 mM sodium chloride [pH 8.0]) supplemented with 2 mM magnesium chloride to chelate the EDTA. The diluted lysate was passed over chelating Sepharose (GE Healthcare, Piscataway, NJ) charged with cobalt(II) chloride and equilibrated in loading buffer. The column was washed with wash buffer (loading buffer plus 30 mM imidazole [pH 8.0]) until protein was no longer detected in the effluent (Bradford assay). The fusion protein was eluted using elution buffer (loading buffer plus 250 mM imidazole). Fractions containing the fusion protein were pooled and dialyzed extensively against dialysis buffer 1 (50 mM Tris [pH 7.5] with 1 mM EDTA [pH 7.5]) in the presence of 1 mg of TEV protease per 50 mg of fusion protein at 4°C (17). After 24 to 72 h, the cleaved fusion protein

was dialyzed for 24 h against dialysis buffer 2 (lacking EDTA). The dialysate was passed over a regenerated cobalt-Sepharose column to remove the His<sub>6</sub>-tagged TEV protease, the His<sub>9</sub>-maltose binding protein (MBP) tag, and uncleaved fusion protein. Pure recombinant mature-length FOX-4 was obtained by passing wash buffer over the column, as FOX-4 has slight affinity for cobalt-Sepharose, and was finally dialyzed against 50 mM Tris (pH 7.5). The final recombinant FOX-4 protein has a Gly-His-Met tripeptide added to the N terminus compared to the native mature-length protein.

Native FOX-4 was produced by culturing the clinical strain *E. coli* 42015 carrying *bla*<sub>FOX-4</sub> overnight from a saturated starter culture into superoptimal broth (SOB) at 37°C with shaking at 200 rpm. The cells were lysed by a stringent periplasmic fractionation method with 40 mg/liter lysozyme and 1.0 U/ml Benzonase nuclease (Novagen), after which 1 mM EDTA was added. The lysate was centrifuged twice to remove cell debris at 12,500 rpm and 10°C for 10 min and filter-sterilized using a 0.22- $\mu$ m-pore-size filter. The lysate was incubated with 5 ml of *m*-aminophenylboronic acid (*m*APBA) agarose, prepared as described previously (18). The mixture was added to a column, the flowthrough was removed (flow rate, 0.3 ml/min), and the column was washed with loading buffer (25 mM Tris and 500 mM sodium chloride [pH 7.0]). Pure FOX-4 was eluted from the

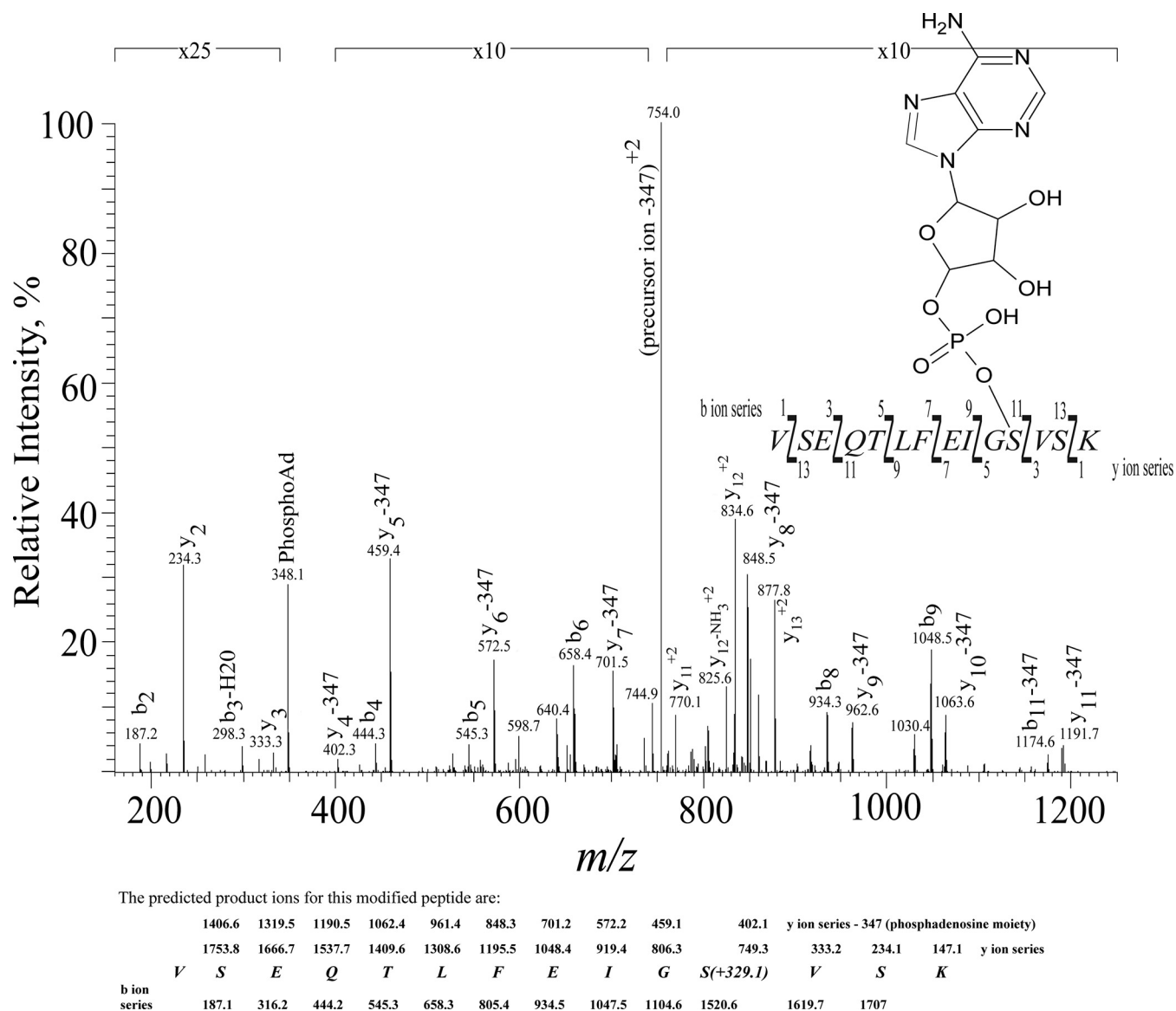


FIG 3 MS/MS spectrum of the FOX-4 triply charged tryptic peptide 55 to 68 (VSEQLTLEIGSVSK) at  $m/z$  618.39. Peptides containing phosphoadenosine (PhosphoAd) display the characteristic neutral loss of 347.1 Da. The ion at  $m/z$  754.0 represents the doubly charged phosphadenosine neutral loss from the precursor ion. The matching b- and y-ion series are labeled.

column using elution buffer (500 mM sodium borate [pH 7.0] and 500 mM sodium chloride). The eluted protein was approximately 95% pure on a Coomassie-stained SDS-PAGE gel. FOX-4 was extensively dialyzed against 50 mM Tris (pH 7.5) and concentrated to 10 mg/ml for the crystallization trials. Protein for kinetics was stored at  $-80^{\circ}\text{C}$ .

**Sample preparation and Nano UPLC-MS/MS analysis.** Twenty-five micrograms of purified FOX-4 protein in 50 mM ammonium bicarbonate ( $\text{NH}_4\text{HCO}_3$ ) (Sigma, USA)–0.01% ProteaseMAX (Promega, USA) was reduced with 5 mM Tris(2-carboxyethyl)phosphine (TCEP) (Thermo, USA) for 30 min at  $25^{\circ}\text{C}$ , followed by alkylation with 25 mM iodoacetamide (Sigma, USA) for 30 min at  $25^{\circ}\text{C}$  in the dark. The sample was then digested with trypsin (Trypsin Gold; Promega) at a ratio of 1:100 at  $37^{\circ}\text{C}$  in a shaker for 3 h. After 3 h of digestion, an aliquot was taken and diluted 50 times with 2% acetonitrile (Fisher, USA)–0.1% trifluoroacetic acid (TFA) (Pierce, USA), and a fraction was analyzed by Nano ultrahigh-performance liquid chromatography–tandem mass spectrometry (UPLC-MS/MS).

$\text{C}_{18}$  reverse-phase (RP) Nano UPLC-MS/MS analysis was performed using a linear ion trap LTQ-XL mass spectrometer (Thermo/Finnigan, USA) connected to a Dionex rapid separation LC (RSLC) UPLC system (Thermo, USA).

The MS/MS raw data file was converted to a Mascot generic format file using Proteome Discoverer version 1.3. A protein database search was performed using Mascot (version 2.4.1) against the taxonomy of all entries or *E. coli* of the NCBI database using the following search parameters: trypsin, two missed cleavages, peptide charges of +2 and +3, peptide tolerance of 2 Da, MS/MS tolerance of 0.6 Da. A decoy database search was also performed to measure the false-discovery rate, carbamidomethylation on cysteine as a fixed modification and variable modifications of deamidation on asparagine and glutamine residues, oxidation on methionine, and phosphoadenosine on histidine, lysine, threonine and tyrosine. The identified phosphoadenylated peptide by Mascot had a low ion score (probability score used to evaluate experimental data versus theoretical) at a threonine residue. Further evaluation of the MS/MS data

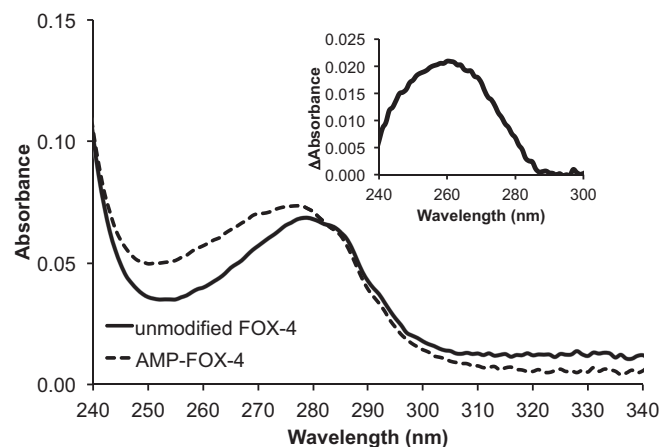


**FIG 4** UV-difference spectrum of adenylylated and unmodified FOX-4. Absorption spectra were collected for concentration-matched ( $A_{280}$ ) samples from the *m*APBA column flowthrough (adenylyl-FOX-4) and elution (unmodified FOX-4) that had been dialyzed into 25 mM Tris (pH 7.5). Inset: difference spectrum showing absorption due to the presence of adenylyl-S64.

localized the phosphoadenylylated residue to a serine residue instead of threonine.

**UV difference spectroscopy.** The *m*APBA column flowthrough (100% adenylylated FOX-4) and eluted protein (100% unmodified FOX-4) were dialyzed overnight against 100 volumes of 25 mM Tris (pH 7.5). The absorption spectra of concentration-matched (1.5  $\mu$ M) samples were measured in the 200- to 350-nm range on a Cary 300 spectrophotometer (Agilent Technologies). The spectrum of the unmodified FOX-4 was subtracted from that of the adenylylated FOX-4. The resulting UV difference spectrum exhibited a maximum absorption at 260 nm.

**Molecular modeling of FOX-4 with adenylylate.** The adenylylate was modeled into the FOX-4 structure bound with the SM23 inhibitor (our unpublished data) using the inhibitor to guide the orientation of the phosphate group. The model was optimized by using Discovery Studio 4.1 software (Accelrys, San Diego, CA). The acyl-enzyme complex was created by making a bond with Ser64, and the CHARMM force field was applied. The FOX-4 coordinates were placed in a fixed atom constraint for energy minimization using steepest descent and conjugate gradient until the minimum convergence with a generalized Born with molecular volume (GBMV) solvation model. Following equilibration, molecular dynamics simulations (substance-volume-temperature [NVT], 300 K) were carried out on the bound ligand with the protein constrained, and the lowest energy conformation was selected. The protein constraints were removed, and the complex was further minimized until convergence.

**X-ray crystallography.** Diffraction-quality crystals for FOX-4 and the Y150F variant were grown by sitting drop vapor diffusion by mixing 1  $\mu$ l of protein (concentration, 15 mg/ml in 50 mM Tris-HCl [pH 7.5]) with 1  $\mu$ l of reservoir solution and equilibrating the samples against the corresponding reservoir solution. The reservoir solution contained 0.05 M zinc acetate and 20% polyethylene glycol 3350 (PEG 3350). Crystals with dimensions of 0.1 mm by 0.1 mm by 0.2 mm were mounted in cryo-loops directly from the crystallization droplet and flash-cooled in liquid nitrogen. Prior to freezing, 20% glycerol was added to the drop as a cryoprotectant. The structure of the complex with cefoxitin was obtained by soaking crystals with a saturating concentration of cefoxitin in the drop. Diffraction data were recorded on a Rayonix 225 high-efficiency (HE) CCD detector (Rayonix LLC, Evanston, IL, USA) with 0.979-Å wavelength radiation on the LRL-CAT beamline (Advanced Photon Source, Argonne, IL). Intensities were integrated using the HKL-2000 program and reduced to amplitudes using the Scalepack2MTZ program (see Table 1 for statistics) (19, 20). All structures were solved using molecular replacement with *Phaser* (21) and the Protein Data Bank (PDB) ID 1ZKJ

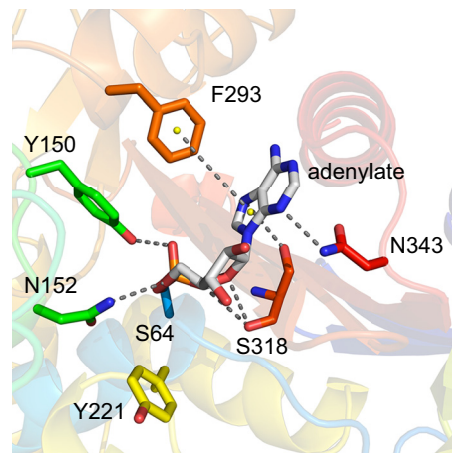


**FIG 5** Model of adenylyl-FOX-4. Adenylylate was manually positioned in FOX-4 using the FOX-4/SM23 boronic acid transition state analogue structure (unpublished data) to guide the placement of phosphate prior to energy minimization. Gray dashes indicate polar contacts, and yellow dashes indicate  $\pi$ - $\pi$  interactions.

structure as a starting model. Final model building and refinement were performed with the programs Coot, Refmac, and Phenix, respectively (22–24). The quality of the final structures was verified with composite omit maps, and stereochemistry was checked with the program MolProbity (25). The Lsqkab and secondary-structure matching (SSM) algorithms were used for structural superpositions (26, 27). All other calculations were conducted using the CCP4 program suite (19).

**Steady-state kinetics.** Steady-state kinetics were carried out on a Cary 300 UV-Vis spectrophotometer (Agilent, Palo Alto, CA), as described previously (28). Briefly, substrate(s) was dissolved in 10 mM phosphate-buffered saline (PBS) (pH 7.4). Enzyme stocks were diluted into PBS containing 0.1 mg/ml bovine serum albumin (Pierce, USA) to improve stability. Velocity-versus-substrate concentration data were fit to the Henri-Michaelis-Menten equation  $v = V_{\max}[S]/(K_m + [S])$  using KaleidaGraph (Synergy Software). For some “slow substrates,” the  $K_m$  was estimated as the competitive inhibition constant  $K_i$  using nitrocefin (NCF) as the reporter substrate. In those cases, the true  $K_i$  was estimated using the equation  $K_i = K_{i\text{ app}} \times (1 + [\text{NCF}]/K_{\text{mNCF}})$ .

## RESULTS

**Two mass isoforms of recombinant FOX-4.** Initially, crystals of recombinantly expressed FOX-4 failed to diffract, so a mass spectrum of the protein was undertaken to determine a cause. The matrix-assisted laser desorption/ionization–time of flight (MALDI-TOF) mass spectrometric analysis revealed two peaks, one at the expected mass and a prominent mass peak at the expected mass + (329  $\pm$  8) Da (29), corresponding to the molecular weight of an adenylylate (AMP) PTM (30, 31). The same phenomenon was observed in three separate purifications of FOX-4 in different laboratories, all bearing different N-terminal tags that were proteolytically removed (His<sub>6</sub>, glutathione *S*-transferase, or His<sub>9</sub>-maltose binding protein). Notably, all constructs lacked the N-terminal signal sequence that specifies periplasmic localization.

To verify the identity and location of the PTM, electrospray ionization-tandem mass spectrometry (ESI-MS/MS) was carried out on a tryptic digest of one of the constructs. Only one peptide, from positions 55 to 68 (VSEQLFEIGSVSK) ( $m/z$  618.4), was observed to bear the additional mass of phosphoadenosine (329.1 Da) (Fig. 3). The MS/MS spectrum for this peptide included the characteristic neutral loss of the phosphoadenosine moiety (31).

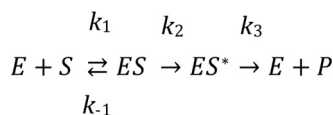


**FIG 6** The reaction proceeds through the reversible formation of the Henri-Michaelis complex ( $ES$ ), followed by acylation to form a covalent intermediate ( $ES^*$ ) and deacylation to yield product ( $P$ ). In general, class C enzymes are deacylation rate limited, so the steady-state rate constant  $k_{\text{cat}}$  approximates  $k_3$  (34).

AMP has been observed as a PTM on histidine, lysine, threonine, and tyrosine residues (32). However, neither the b- nor the y-ion series bearing threonine or lysine gave a pattern reflecting adenylation there. This was also reflected in the low Mascot ion score obtained, since only His, Lys, Thr, and Tyr are listed as the possible amino acid residues for this PTM. Another possibility was one of the three serine residues (Ser56, Ser64, or Ser66). Examination of the MS/MS spectrum revealed that the amino acid residues VSEQTLFEIG were all unmodified from the matching  $b_{2-10}$  series and that residues VSK were also unmodified from the matching  $y_{2-3}$  series. The  $y_{4-10}$  series all contained the neutral loss of the phosphoadenosine moiety (31). Therefore, the MS/MS spectrum (Fig. 3) fragmentation pattern strongly supports the localization of the phosphoadenosine PTM to Ser64: VSEQTLFEIG S(phosphoadenosine)VSK.

The identity and location of the PTM are also borne out by functional studies on the adenylylated protein. The modified and unmodified FOX-4 proteins can be separated using *mAPBA* agarose. The boronic acid functionality covalently binds to the unmodified protein on the S64 residue, while the modified protein passes through the column. The modified protein (flowthrough) does not demonstrate detectable activity against nitrocefin, suggesting that the AMP group blocks the active site, while the unmodified protein (eluted with sodium borate) is strongly active (data not shown). The UV spectrum of the modified protein has a stronger absorption than the unmodified protein in the 240- to 300-nm range (Fig. 4). The difference spectrum (Fig. 4, inset) reveals the absorption spectrum of the PTM, with an absorption peak at 260 nm corresponding to adenylate. The magnitude of this absorption is consistent with a stoichiometry of one AMP group per protein ( $\epsilon_{260} = 15,300 \text{ M}^{-1} \text{ cm}^{-1}$  for adenylate). Phosphodiesterase I (from *Crotalus atrox*) treatment removes the AMP group from the protein in a time-dependent manner, as assessed by mass spectrometry (data not shown).

The S64A substitution generates a FOX-4 protein of a single mass that also produces diffracting crystals. Unmodified wild-type FOX-4 was ultimately obtained by its expression in the clinical *E. coli* strain Ec GCE (33), followed by purification using the *mAPBA* resin, which binds to S64 and excludes the modified enzyme. The high yield of unmodified protein suggests that adenylation occurs sparingly (if at all) in the native host, perhaps owing to the periplasmic localization sequence that is missing in the recombinant tagged protein. The recombinant Y150F variant, which generally halts catalysis at the acyl-enzyme intermediate, is also unmodified despite being cytoplasmically expressed. The lack of PTM in this variant suggests that an intact  $\beta$ -lactamase catalytic center is required for the modification. Finally, a model of FOX-4 with AMP bound to S64 suggests the possibility of hydrogen bonding to N152, Y150, S318, and N343 in the active site and no

steric clashes (Fig. 5). A putative T-shaped  $\pi$ -stacking interaction between F293 and the adenine ring might provide a rationale for the unique adenylation of FOX-4 (and not other class C enzymes), because the substitution of phenylalanine at that position is observed in the FOX family only.

**Steady-state kinetics of unmodified FOX-4.** Previous efforts to characterize FOX-4 have relied on recombinant expression of the protein using affinity tags. As the PTM state of the protein was not known, the *in vitro* kinetics for a few compounds was carried out to compare to previous studies. The catalytic mechanism of  $\beta$ -lactamase is seen in Fig. 6. The  $k_{\text{cat}}$  and  $K_m$  values obtained in this study (Table 2) were similar to those from a previous study (14). Compared to other class C enzymes, FOX-4 has a much higher  $k_{\text{cat}}$  when hydrolyzing cefoxitin. Similarly, FOX-4 displays relatively higher  $k_{\text{cat}}$  values for cefotaxime and ceftazidime. Enzymes that are designated cephamycinases display considerably higher  $k_{\text{cat}}$  values (deacylation) than those of noncephamycinases, with the exception of *E. coli* K-12 AmpC, for which acylation may also be impaired (34). Notably, compared to FOX-4, plasmid-mediated enzymes ACT-1 and MIR-1 also exhibit relatively high  $k_{\text{cat}}$  values for cefoxitin of  $0.37 \text{ s}^{-1}$  and  $0.64 \text{ s}^{-1}$ , respectively (35). The  $K_m$  values for poor cephalosporin substrates are quite low ( $0.004 \text{ }\mu\text{M}$  to  $4 \text{ }\mu\text{M}$ ); thus, the  $K_m$  values are likely a physiologically relevant factor for the hydrolysis of these  $\beta$ -lactams, as is  $k_{\text{cat}}$ .

**X-ray structures of wild-type FOX-4, Y150F, and Y150F-cefoxitin complex.** (i) **Apo structures.** The wild-type FOX-4 shows a typical class C fold with an  $\alpha$ -helical region and a mixed  $\alpha$ -helix/ $\beta$ -sheet region (Fig. 7). The refinement statistics are shown in Table 1. All residues are within allowed Ramachandran regions. Importantly, electron density was observed for all regions of the protein; in the crystal structures of the closely related enzymes, the  $\Omega$  loop and/or R2 loop region are missing electron density for a few residues (MOX-1, residues 214 and 215 and 303 to 306; CMY-

**TABLE 2** Initial-rate kinetics of native wild-type FOX-4 and other class C enzymes

Enzyme by drug	$K_m$ ( $\mu\text{M}$ )	$k_{\text{cat}}$ ( $\text{s}^{-1}$ )	$k_{\text{cat}}/K_m$ ( $\mu\text{M}^{-1}\text{s}^{-1}$ )
<b>Cefoxitin</b>			
FOX-4 <sup>a</sup>	$0.11 \pm 0.01$	$0.91 \pm 0.06$	$8.3 \pm 0.9$
<i>P. aeruginosa</i> AmpC <sup>b</sup>	0.05	0.12	2.4
CMY-2 <sup>c</sup>	0.07	0.23	3.3
<i>C. freundii</i> AmpC <sup>b</sup>	0.25	0.032	1.3
K-12 AmpC <sup>b</sup>	0.65	0.2	0.3
P99 AmpC <sup>b</sup>	0.024	0.06	2.5
<b>Cefotaxime</b>			
FOX-4	$0.12 \pm 0.01$	$0.47 \pm 0.01$	$3.9 \pm 0.1$
<i>P. aeruginosa</i> AmpC <sup>b</sup>	0.2	0.15	0.75
CMY-2 <sup>c</sup>	0.004	0.0012	3.3
<i>C. freundii</i> AmpC <sup>b</sup>	0.005	0.017	3.4
K-12 AmpC <sup>b</sup>	1.7	0.17	0.1
P99 AmpC <sup>b</sup>	0.01	0.015	1.5
<b>Ceftazidime</b>			
FOX-4 <sup>a</sup>	$4.1 \pm 0.1$	$0.30 \pm 0.01$	$0.073 \pm 0.001$
P99 AmpC <sup>d</sup>	4	0.012	0.003

<sup>a</sup> Data from this study.

<sup>b</sup> Data from Galleni et al. (34).

<sup>c</sup> Data from Bauvois et al. (35).

<sup>d</sup> Data from Matagne et al. (41).

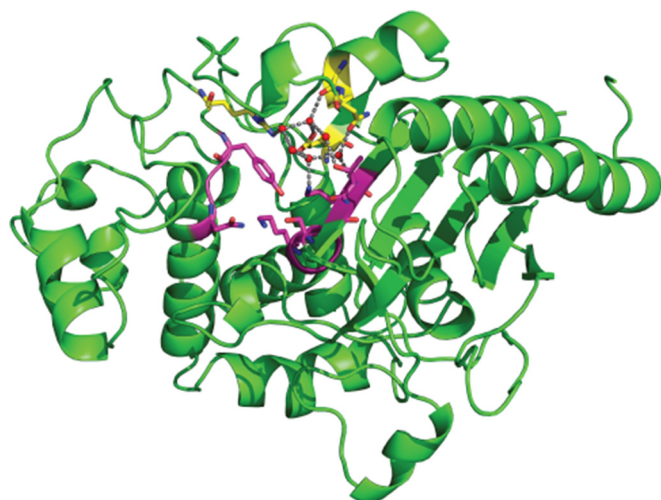


**FIG 7** Crystal structure of apo-FOX-4 (1.6 Å) shows a cluster of water molecules (red spheres) interacting with residues R148, E272, G286, and N287 (yellow). Conserved active-site motif side chains are shown for SXXX<sub>64–67</sub>, YXN<sub>150–152</sub>, and KTG<sub>315–317</sub> (magenta). This image and those that follow were made using PyMOL (Schrödinger).

10, residues 304 to 306). At 1.6-Å refinement, several ordered water molecules were seen in the active site contacting the residues R148, E272, G286, and N287 (Fig. 7, yellow shading).

The Y150F protein crystallized with two monomers per asymmetric unit in space group P2<sub>1</sub>. The overall structure is substantially the same as that of wild-type FOX-4, except for slight shifts in some side chain positions (Fig. 8). F293 has rotated ~60° and has shifted 4.1 Å. The phenol ring of Y221 has shifted 1.9 Å. Other changes are more subtle and will be considered below.

**(ii) FOX-4-cefoxitin structure.** The deacylation-deficient Y150F variant was used to trap the acyl-enzyme intermediate of cefoxitin. The Y150F crystals were soaked with cefoxitin. The soaked crystals diffracted to 1.2 Å, with one monomer and two cefoxitin molecules per asymmetric unit. One of the cefoxitin molecules was captured in the active site, and the electron density shows that the β-lactam ring carbonyl was contiguous with S64 and that the carboxamide R2 side chain was eliminated (Fig. 9).

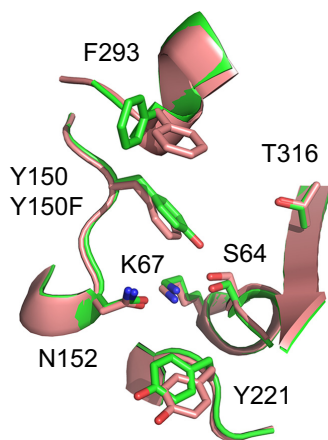


**FIG 8** Overlay of wild-type FOX-4 (green) and Y150F FOX-4 (pink) apo crystal structures.

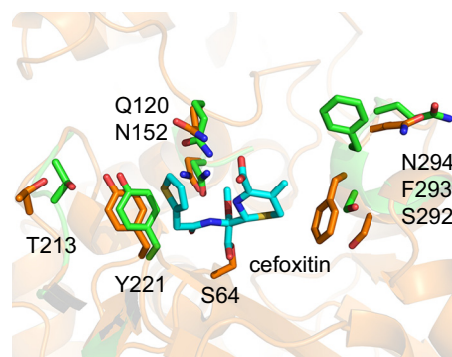


**FIG 9** Overlay of wild-type FOX-4 (green) and Y150F FOX-4-acyl-cefoxitin (orange) crystal structures.

The second cefoxitin bound in a region below the Ω loop (near E171 and Q190) and appeared to be intact; the significance of this finding is unknown at this time (data not shown).

The most prominent change in the acyl-enzyme, compared to both apo structures, is a reorganization of the R2 loop/helix H10 (P289 to N297) (Fig. 10A). The most dramatic movement is in F293, whose side chain rotates 130°, causing a 10.3-Å (7.6 Å from Y150F apo) shift in the position of the phenyl ring. The Cα atom moves 2.5 Å toward the substrate and comes within 3.5 Å of the dihydrothiazine ring sulfur. Neighboring S292 and N294 also rearranged their side chains by 154° and 4.1 Å and 135° and 5.6 Å, respectively, compared to the wild-type apo structure. The significance of these movements is not readily apparent, as they do not appear to form new polar contacts. The space occupied by the repositioned F293 side chain presumably contained the substrate R2 carboxamide prior to its elimination.

Also notable are new polar contacts that are formed in the acyl-cefoxitin structure (Fig. 9). The hydrogen bond between the N152 and Q120 side chains is broken upon ligand binding, with N152 rotating 1.7 Å away to prevent a steric clash with the 7-α-methoxy group of cefoxitin (3.5 Å separates the methyl group and the N152 side chain). The Q120 side chain moves 2.2 Å to form a hydrogen bond to the substrate C<sub>4</sub> carboxylate, which appears far from its usual binding pocket near residues N343 and I346.

While the new contacts mentioned above seem to clearly impact binding and catalysis, the purpose of other new contacts is less obvious. A potentially significant interaction seen only in the liganded structure and not in either apo structure is the hydrogen bond between E171 and Q190 (perhaps related to the second cefoxitin molecule).

More subtle changes in the backbone conformation between wild-type apo and Y150F-cefoxitin complex are seen in the Ω loop (G202 to G215), occurring in two segments (Fig. 10B). Compared to their positions in the wild-type apo enzyme, the K205 side chain is displaced by 5.8 Å, the E206 Cα moves 1.9 Å, the D207 Cα moves 1.9 Å, and the K208 side chain is displaced by 1.5 Å. Residues P209 to R211 align well in both structures, but residues A212 to P214 have backbone shifts of about 2.0 Å. An N-terminal loop (L33 to N42) also shows a 2.3-Å shift in the position of its Cα atoms.

The differences between the Y150F apo and Y150F-cefoxitin complex structures are minimal, since the ligand was soaked into the Y150F crystal. Cefoxitin causes only a subtle change in the Ω loop, focused on the T213 side chain that moves 2.9 Å (and Cα

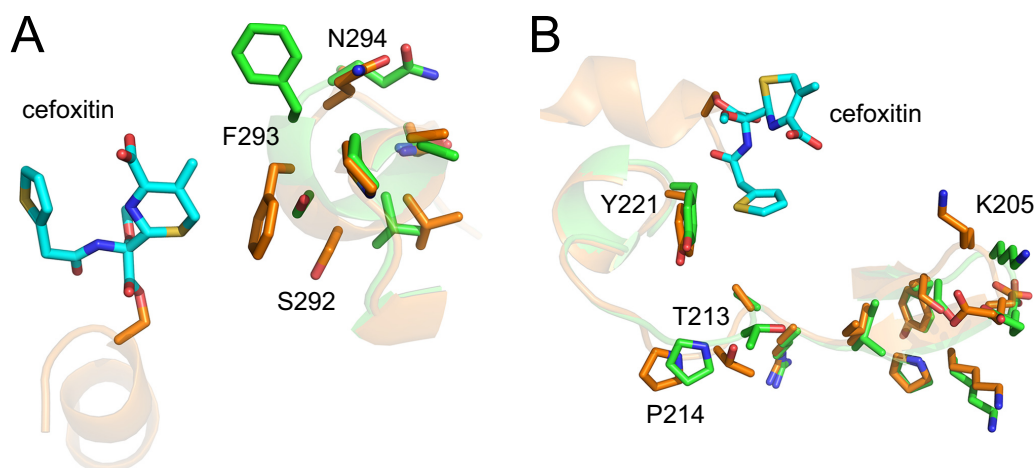


FIG 10 Structural changes in loops upon cefoxitin binding. Wild-type FOX-4, green; Y150F FOX-4–cefoxitin, orange. (A) R2 loop. (B)  $\Omega$  loop.

moving 2.2 Å) away from the substrate thiophene ring. To maximize edge-to-face  $\pi$ -stacking interactions with this ring, Y221 also shifts by 1.4 Å. Again, the F293 side chain rotation toward the substrate is the most significant structural difference between the apo and liganded structures. This position is conserved in AmpC as a leucine; several FOX family members are the only AmpC enzymes that replace this residue with phenylalanine.

## DISCUSSION

FOX-type plasmid-based AmpC cephamycinases, while less commonly observed than CMY-type AmpC, are clinically important resistance enzymes (36, 37). We present here for the first time the structure of a member of the FOX family, FOX-4. The structures of the apo- and cefoxitin-bound enzymes show minor differences that do not make the mechanism of rate enhancement against cefoxitin readily apparent. Movement in the R2 loop (helix H10) residue F293 upon substrate binding suggests a rearrangement in this region that may impact catalysis. FOX family members differing at this position, FOX-3 (Phe) and FOX-8 (Leu), show differences in substrate selectivity (38). Other class C enzymes have a leucine at this position, so the larger phenylalanine may impact substrate repositioning.

The most striking difference among structures of acylated class C enzymes is the positioning of the dihydrothiazine ring common to all cephalosporins. Structural comparisons of extended-spectrum enzymes FOX-4 and MOX-1 with non-extended-spectrum *E. coli* AmpC  $\beta$ -lactamase reveal two principal motions of this ring that correspond to characteristic features in the active site and, importantly, distinguish cephamycin-resistant and -susceptible enzymes.

The first motion, rotation about the C<sub>7</sub>–C<sub>8</sub> bond, must be accomplished to tilt the dihydrothiazine ring away from the R2 substrate-binding loop. This rotation also causes the cephamycin 7- $\alpha$ -methoxy group to impinge on the N152 side chain, requiring a shift in its position. The second motion, rotation about the C<sub>6</sub>–C<sub>7</sub> bond, moves the C<sub>4</sub> carboxylate either into a substrate- or product-like conformation (hydrogen bonded to N343/N346 or Q120, respectively).

The wild-type AmpC structure with acyl-moxalactam (PDB ID 1FCO) shows neither of these motions. The first rotation is steri-

cally blocked by N152, but it appears that the N152A substitution (PDB ID 1I5Q) allows the rotation to occur due to the relief of steric hindrance (Fig. 11A). The second rotation is blocked for both acyl-moxalactam AmpC structures because of charge repulsion between the C<sub>4</sub> carboxylate and the R1 side chain carboxylate.

The wild-type AmpC structure with acyl-cephalothin (PDB ID 1KVM) shows that the first motion can occur (due to lack of steric hindrance with N152) and the second rotation has partially occurred (Fig. 11B). In general, the C<sub>4</sub> carboxylate seems to hydrogen bond directly to either N346 (moxalactam) or N343 (cephalothin), interacting indirectly with another Asn residue through a bridging water molecule. However, neither of these conformations resembles that of the enzyme-product complex. In the cephalothin product-AmpC complex (PDB ID 1KVL), both motions have fully occurred, with the C<sub>4</sub> carboxylate having rotated some 120° to hydrogen bond directly to Q120 (Fig. 11C).

In the FOX-4 Y150F–acyl-cefoxitin structure (PDB ID 5CGX), the ring can accomplish both motions and adopts a conformation nearly identical to that of the cephalothin product, with the C<sub>4</sub> carboxylate hydrogen bonded to Q120. Notably, FOX-4 lacks the hydrogen-bonded network in the position 343 to 346 region due to the N346I and N289P substitutions, relative to AmpC (Fig. 9D). Likewise, in the AmpC N152G–acyl-cefoxitin structure (PDB ID 4KEN), the ring accomplishes both motions. The N152G mutation prevents the expected steric clash with the 7- $\alpha$ -methoxy group but possibly reduces substrate turnover (cf. N152G in AmpC from *E. cloacae* P99 [39]).

The structural features that permit cephamycin hydrolysis in FOX-4 but not in *E. coli* AmpC may now be rationalized as follows. The first motion of the dihydrothiazine ring (about C<sub>7</sub>–C<sub>8</sub>) is able to occur in both FOX-4 and AmpC N152G–acyl-cefoxitin structures due to a slight widening of the active-site pocket. In FOX-4 (and MOX-1), this widening appears to be achieved through the S153P substitution. The proline subtly alters the backbone conformation, moving N152 0.7 Å further away from the substrate in FOX-4 than it is in AmpC. Presumably, this shift provides enough room for the 7- $\alpha$ -methoxy and amide side chain to rearrange. In AmpC, the observed rearrangement of cefoxitin (PDB ID 4KEN) is facilitated by the N152G mutation, which provides adequate space. The second motion of the dihydrothiazine

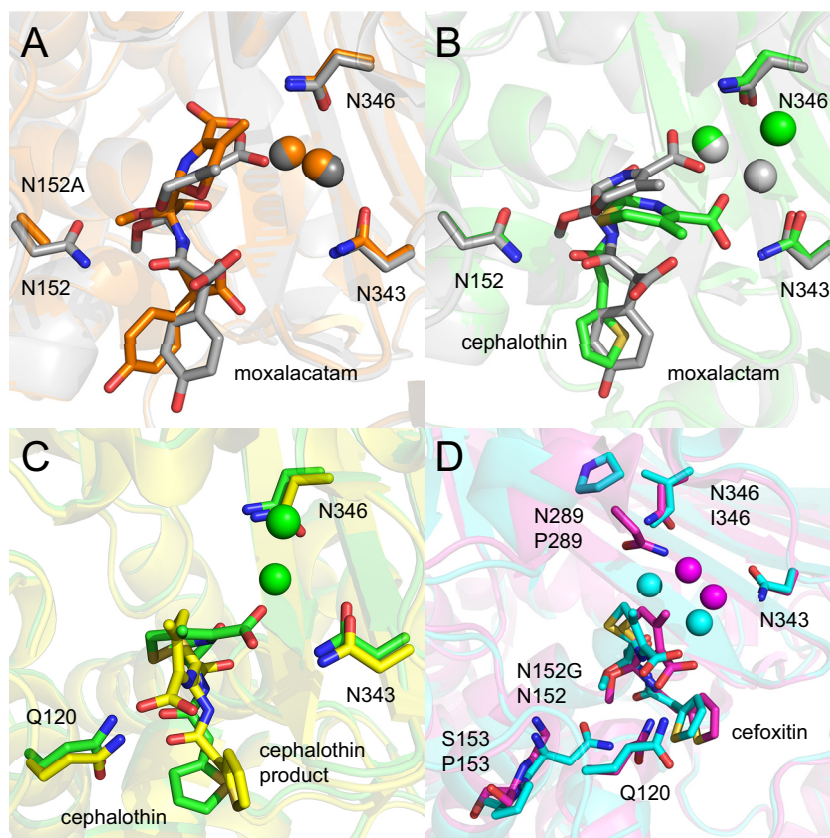


**FIG 11** Overlays of cephalosporins and cephamycins in class C  $\beta$ -lactamases. (A) Moxalactam in *E. coli* AmpC (wild type, PDB ID [1FCO](#) chain B, gray; N152A, PDB ID [1I5Q](#) chain B, orange). (B) Moxalactam (PDB ID [1FCO](#), gray) and cephalothin (PDB ID [1KVM](#), green) in wild-type *E. coli* AmpC. (C) Acyl-cephalexin (PDB ID [1KVM](#), green) and cephalothin product (PDB ID [1KVL](#), yellow) in wild-type *E. coli* AmpC. (D) Cefoxitin in FOX-4 (Y150F, PDB ID [5CGX](#), this work, cyan) and *E. coli* AmpC (N152G, PDB ID [4KEN](#), magenta).

ring (about C<sub>6</sub>—C<sub>7</sub>) is facilitated in FOX-4 by the substitution of Ile at position 346, which disrupts the hydrogen-bonded network in the usual C<sub>4</sub>-carboxylate binding region. The ability of cefoxitin to evade interactions with N343/N346 in the AmpC structure and accomplish the full C<sub>6</sub>—C<sub>7</sub> rotation is not explained well by this hypothesis and requires further investigation.

The rotation of the dihydrothiazine ring, first seen in the *E. coli* AmpC—cephalexin product structure and now observed in the acyl-cefoxitin structures of FOX-4 Y150F and AmpC N152G, points to this motion as being important for progress through the reaction. The ability of FOX-4 to promote a product-like geometry for cefoxitin may account for its considerable deacylation rate enhancement. The FOX-4 binding pocket has several substitutions relative to *E. coli* AmpC, including S153P near the catalytic N152 residue and N289P and N346I in the carboxylate-binding region. The S153P substitution is common to all of the extended-spectrum enzymes, except CMY-2, and may be a common strategy for accommodating bulky substrates ([Fig. 2](#)). Positions 289 and 346 form hydrogen bonds in *E. coli* AmpC but not in FOX-4. Since FOX-4 lacks a polar side chain to position the bridging water molecule, it has no means by which to bind the carboxylate in that region. The same substitution is seen in MOX-1 and CMY-10, and it has been shown that mutations at position 346 alter specificity toward carbapenems in many plasmid-based class C enzymes ([15](#)). It remains to be seen whether FOX enzymes are similarly affected.

Our investigation of FOX-4 has serendipitously uncovered a novel PTM in  $\beta$ -lactamases: the adenylation of a serine residue. Previously, only histidine, tyrosine, threonine, and lysine have been shown to be adenylated ([32](#)). The modification is observed in bacteria as part of a nutrient-sensing system involving glutamine synthase, but it is little seen elsewhere. This first example of a serine modification differs from the others in several ways. First, it is probably artifactual rather than functional, given that it blocks the active site of the enzyme and seems unlikely to serve an evolutionary role. Only cytoplasmically expressed proteins appear to be modified, while those that are exported to the periplasm escape modification. Second, it is unlikely to be mediated by an adenylyltransferase. The active site is sterically hindered, so the folded enzyme could not receive the modification. While the modification might be added prior to folding, this too seems unlikely, as distal mutations (Y150F and Y150E) completely ablate it. It seems more likely that some adenylate donor fits into the FOX-4 active site and, due to the strong nucleophilicity of S64, is attacked. The same phenomenon is observed for designed phosphonate inhibitors ([40](#)). Phospho-S64 was recently observed in the MOX-1 structure (PDB ID [3W8K](#)). While the FOX-4 AMP donor is unknown, it seems reasonable that an aminoacyl-AMP complex, such as that used for protein synthesis, might be a substrate, or even cAMP.

While the mixture of modified and unmodified protein initially stymied structure determination efforts, the presence of

the AMPylation raises certain questions. Could analogues of adenylate donors be used as inhibitors? Is this modification seen only in FOX enzymes, or does it appear in other recombinantly expressed  $\beta$ -lactamases? These questions highlight the need for new compounds and new approaches to stop the progression of antibiotic resistance. Nevertheless, the present work reveals the first structure of a FOX family cephamycinase, providing insight into the evolution of substrate selectivity in class C  $\beta$ -lactamases.

## FUNDING INFORMATION

HHS | National Institutes of Health (NIH) provided funding to Vladimir N. Malashkevich, Steven C. Almo, and Robert A. Bonomo under grant numbers AI100560, AI063517, GM094662, 1S10RR029398, and 1S10RR019352. U.S. Department of Veterans Affairs (VA) provided funding to Robert A. Bonomo under grant number BX001974. DOE | Argonne National Laboratory, Office of Science (ANL) provided funding to Vladimir N. Malashkevich and Steven C. Almo under grant number DE-AC02-06CH11357.

Crystallographic and mass spectrometric efforts were provided by the NYSGRG, which is supported by NIGMS grant no. U54 GM094662 to S.C.A. Mass spectrometry was also supported by grants NIH SIG 1S10RR029398 (Orbitrap) and 1S10RR019352 (LTQ). This research used resources of the Advanced Photon Source, a U.S. Department of Energy (DOE) Office of Science User Facility operated for the DOE Office of Science by Argonne National Laboratory under contract DE-AC02-06CH11357. Use of the Lilly Research Laboratories Collaborative Access Team (LRL-CAT) beamline at sector 31 of the Advanced Photon Source was provided by the Eli Lilly Company, which operates the facility. R.A.B. is supported in part by funds and/or facilities provided by the Cleveland Department of Veterans Affairs and the Veterans Integrated Service Network 10 Geriatric Research, Education, and Clinical Center (VISN 10 GRECC). K.M.P.-W. is supported in part by funds and/or facilities provided by the Cleveland Department of Veterans Affairs and by the Veterans Affairs Merit Review Program Award 1101BX002872. S.T.L. is supported by a Hofstra University Faculty Research and Development Grant.

## REFERENCES

1. Stapley EO, Jackson M, Hernandez S, Zimmerman SB, Currie SA, Mochales S, Mata JM, Woodruff HB, Hendlin D. 1972. Cephamycins, a new family of  $\beta$ -lactam antibiotics. I. Production by actinomycetes, including *Streptomyces lactamdurans* sp. n. *Antimicrob Agents Chemother* 2:122–131.
2. Birnbaum J, Stapley EO, Miller AK, Wallick H, Hendlin D, Woodruff HB. 1978. Cefoxitin, a semi-synthetic cephamycin: a microbiological overview. *J Antimicrob Chemother* 4:15–32. [http://dx.doi.org/10.1093/jac/4.suppl\\_B.15](http://dx.doi.org/10.1093/jac/4.suppl_B.15).
3. Stapley EO, Birnbaum J, Miller AK, Wallick H, Hendlin D, Woodruff HB. 1979. Cefoxitin and cephamycins: microbiological studies. *Rev Infect Dis* 1:73–89. <http://dx.doi.org/10.1093/clinids/1.1.73>.
4. Taylor G, Blondel-Hill E, Kibsey P, Friesen E, Tisdell R, Vaudry W. 1993. Containing cefoxitin costs through a program to curtail use in surgical prophylaxis. *Can J Infect Dis* 4:275–278.
5. Bieluch VM, Cuchural GJ, Snyderman DR, Gorbach SL, Tally FP. 1987. Clinical importance of cefoxitin-resistant *Bacteroides fragilis* isolates. *Diagn Microbiol Infect Dis* 7:119–126. [http://dx.doi.org/10.1016/0732-8893\(87\)90029-0](http://dx.doi.org/10.1016/0732-8893(87)90029-0).
6. Hashizume T, Yamaguchi A, Sawai T. 1986. Outer membrane permeability of imipenem in comparison with other beta-lactam antibiotics. *J Antibiot (Tokyo)* 39:153–156. <http://dx.doi.org/10.7164/antibiotics.39.153>.
7. Mulvey MR, Bryce E, Boyd DA, Ofner-Agostini M, Land AM, Simor AE, Paton S, Canadian Hospital Epidemiology Committee, Canadian Nosocomial Infection Surveillance Program, Health Canada. 2005. Molecular characterization of cefoxitin-resistant *Escherichia coli* from Canadian hospitals. *Antimicrob Agents Chemother* 49:358–365. <http://dx.doi.org/10.1128/AAC.49.1.358-365.2005>.
8. Philippon A, Arlet G, Jacoby GA. 2002. Plasmid-determined AmpC-type  $\beta$ -lactamases. *Antimicrob Agents Chemother* 46:1–11. <http://dx.doi.org/10.1128/AAC.46.1.1-11.2002>.
9. Mammeri H, Galleni M, Nordmann P. 2009. Role of the Ser-287-Asn replacement in the hydrolysis spectrum extension of AmpC beta-lactamases in *Escherichia coli*. *Antimicrob Agents Chemother* 53:323–326. <http://dx.doi.org/10.1128/AAC.00608-08>.
10. Rogers BA, Sidjabat HE, Paterson DL. 2011. *Escherichia coli* O25b-ST131: a pandemic, multiresistant, community-associated strain. *J Antimicrob Chemother* 66:1–14. <http://dx.doi.org/10.1093/jac/dkq415>.
11. Mammeri H, Poirel L, Nordmann P. 2007. Extension of the hydrolysis spectrum of AmpC beta-lactamase of *Escherichia coli* due to amino acid insertion in the H-10 helix. *J Antimicrob Chemother* 60:490–494. <http://dx.doi.org/10.1093/jac/dkm227>.
12. Kim JY, Jung HI, An YJ, Lee JH, Kim SJ, Jeong SH, Lee KJ, Suh PG, Lee HS, Lee SH, Cha SS. 2006. Structural basis for the extended substrate spectrum of CMY-10, a plasmid-encoded class C  $\beta$ -lactamase. *Mol Microbiol* 60:907–916. <http://dx.doi.org/10.1111/j.1365-2958.2006.05146.x>.
13. Gonzalez Leiza M, Perez-Diaz JC, Ayala J, Casellas JM, Martinez-Beltran J, Bush K, Baquero F. 1994. Gene sequence and biochemical characterization of FOX-1 from *Klebsiella pneumoniae*, a new AmpC-type plasmid-mediated  $\beta$ -lactamase with two molecular variants. *Antimicrob Agents Chemother* 38:2150–2157. <http://dx.doi.org/10.1128/AAC.38.9.2150>.
14. Mallo S, Pérez-Llarena FJ, Kerff F, Soares NC, Galleni M, Bou G. 2010. A tripeptide deletion in the R2 loop of the class C  $\beta$ -lactamase enzyme FOX-4 impairs cefoxitin hydrolysis and slightly increases susceptibility to  $\beta$ -lactamase inhibitors. *J Antimicrob Chemother* 65:1187–1194. <http://dx.doi.org/10.1093/jac/dkq115>.
15. Dahyot S, Broutin I, de Champs C, Guillon H, Mammeri H. 2013. Contribution of asparagine 346 residue to the carbapenemase activity of CMY-2  $\beta$ -lactamase. *FEMS Microbiol Lett* 345:147–153. <http://dx.doi.org/10.1111/1574-6968.12199>.
16. Galleni M, Lindberg F, Normark S, Cole S, Honore N, Joris B, Frere JM. 1988. Sequence and comparative analysis of three *Enterobacter cloacae* ampC beta-lactamase genes and their products. *Biochem J* 250:753–760. <http://dx.doi.org/10.1042/bj2500753>.
17. Kapust RB, Tozser J, Fox JD, Anderson DE, Cherry S, Copeland TD, Waugh DS. 2001. Tobacco etch virus protease: mechanism of autolysis and rational design of stable mutants with wild-type catalytic proficiency. *Protein Eng* 14:993–1000. <http://dx.doi.org/10.1093/protein/14.12.993>.
18. Cartwright SJ, Waley SG. 1984. Purification of beta-lactamases by affinity chromatography on phenylboronic acid-agarose. *Biochem J* 221:505–512. <http://dx.doi.org/10.1042/bj2210505>.
19. Winn MD, Ballard CC, Cowtan KD, Dodson EJ, Emsley P, Evans PR, Keegan RM, Krissinel EB, Leslie AG, McCoy A, McNicholas SJ, Murshudov GN, Pannu NS, Potterton EA, Powell HR, Read RJ, Vagin A, Wilson KS. 2011. Overview of the CCP4 suite and current developments. *Acta Crystallogr D Biol Crystallogr* 67:235–242. <http://dx.doi.org/10.1107/S0907444910045749>.
20. Otwinowski Z, Minor W. 1997. Processing of X-ray diffraction data collected in oscillation mode. *Methods Enzymol* 276:307–326. [http://dx.doi.org/10.1016/S0076-6879\(97\)76066-X](http://dx.doi.org/10.1016/S0076-6879(97)76066-X).
21. McCoy AJ, Grosse-Kunstleve RW, Adams PD, Winn MD, Storoni LC, Read RJ. 2007. *Phaser* crystallographic software. *J Appl Crystallogr* 40:658–674. <http://dx.doi.org/10.1107/S0021889807021206>.
22. Adams PD, Afonine PV, Bunkoczi G, Chen VB, Davis IW, Echols N, Headd JJ, Hung LW, Kapral GJ, Grosse-Kunstleve RW, McCoy AJ, Moriarty NW, Oeffner R, Read RJ, Richardson DC, Richardson JS, Terwilliger TC, Zwart PH. 2010. PHENIX: a comprehensive Python-based system for macromolecular structure solution. *Acta Crystallogr D Biol Crystallogr* 66:213–221. <http://dx.doi.org/10.1107/S0907444909052925>.
23. Emsley P, Cowtan K. 2004. Coot: model-building tools for molecular graphics. *Acta Crystallogr D Biol Crystallogr* 60:2126–2132. <http://dx.doi.org/10.1107/S0907444904019158>.
24. Murshudov GN, Vagin AA, Dodson EJ. 1997. Refinement of macromolecular structures by the maximum-likelihood method. *Acta Crystallogr D Biol Crystallogr* 53:240–255. <http://dx.doi.org/10.1107/S0907444996012255>.
25. Chen VB, Arendall WB, III, Headd JJ, Keedy DA, Immormino RM, Kapral GJ, Murray LW, Richardson JS, Richardson DC. 2010. MolProbity: all-atom structure validation for macromolecular crystallography. *Acta Crystallogr D Biol Crystallogr* 66:12–21. <http://dx.doi.org/10.1107/S0907444909042073>.

26. Kabsch W. 1976. A solution for the best rotation to relate two sets of vectors. *Acta Crystallogr A* 32:922–923. <http://dx.doi.org/10.1107/S0567739476001873>.
27. Krissinel E, Henrick K. 2004. Secondary-structure matching (SSM), a new tool for fast protein structure alignment in three dimensions. *Acta Crystallogr D Biol Crystallogr* 60:2256–2268. <http://dx.doi.org/10.1107/S0907444904026460>.
28. Drawz SM, Taracila M, Caselli E, Prati F, Bonomo RA. 2011. Exploring sequence requirements for C<sub>3</sub>/C<sub>4</sub> carboxylate recognition in the *Pseudomonas aeruginosa* cephalosporinase: insights into plasticity of the AmpC  $\beta$ -lactamase. *Protein Sci* 20:941–958. <http://dx.doi.org/10.1002/pro.612>.
29. Papp-Wallace KM, Mallo S, Bethel CR, Taracila MA, Hujer AM, Fernandez A, Gatta JA, Smith KM, Xu Y, Page MG, Desarbre E, Bou G, Bonomo RA. 2014. A kinetic analysis of the inhibition of FOX-4  $\beta$ -lactamase, a plasmid-mediated AmpC cephalosporinase, by monocyclic  $\beta$ -lactams and carbapenems. *J Antimicrob Chemother* 69:682–690. <http://dx.doi.org/10.1093/jac/dkt434>.
30. Li Y, Al-Eryani R, Yarbrough ML, Orth K, Ball HL. 2011. Characterization of AMPylation on threonine, serine, and tyrosine using mass spectrometry. *J Am Soc Mass Spectrom* 22:752–761. <http://dx.doi.org/10.1007/s13361-011-0084-1>.
31. Hansen T, Albers M, Hedberg C, Sickmann A. 2013. Adenylation, MS, and proteomics—introducing a “new” modification to bottom-up proteomics. *Proteomics* 13:955–963. <http://dx.doi.org/10.1002/pmic.201200344>.
32. Itzen A, Blankenfeldt W, Goody RS. 2011. Adenylation: renaissance of a forgotten post-translational modification. *Trends Biochem Sci* 36:221–228. <http://dx.doi.org/10.1016/j.tibs.2010.12.004>.
33. Bou G, Oliver A, Ojeda M, Monzon C, Martinez-Beltran J. 2000. Molecular characterization of FOX-4, a new AmpC-type plasmid-mediated  $\beta$ -lactamase from an *Escherichia coli* strain isolated in Spain. *Antimicrob Agents Chemother* 44:2549–2553. <http://dx.doi.org/10.1128/AAC.44.9.2549-2553.2000>.
34. Galleni M, Amicosante G, Frere JM. 1988. A survey of the kinetic parameters of class C  $\beta$ -lactamases. Cephalosporins and other  $\beta$ -lactam compounds. *Biochem J* 255:123–129.
35. Bauvois C, Ibuka AS, Celso A, Alba J, Ishii Y, Frere JM, Galleni M. 2005. Kinetic properties of four plasmid-mediated AmpC  $\beta$ -lactamases. *Antimicrob Agents Chemother* 49:4240–4246. <http://dx.doi.org/10.1128/AAC.49.10.4240-4246.2005>.
36. Jacoby GA. 2009. AmpC  $\beta$ -lactamases. *Clin Microbiol Rev* 22:161–182. <http://dx.doi.org/10.1128/CMR.00036-08>.
37. Arena F, Giani T, Becucci E, Conte V, Zanelli G, D’Andrea MM, Buonocore G, Bagnoli F, Zanchi A, Montagnani F, Rossolini GM. 2013. Large oligoclonal outbreak due to *Klebsiella pneumoniae* ST14 and ST26 producing the FOX-7 AmpC  $\beta$ -lactamase in a neonatal intensive care unit. *J Clin Microbiol* 51:4067–4072. <http://dx.doi.org/10.1128/JCM.01982-13>.
38. Pérez-Llarena FJ, Kerff F, Zamorano L, Fernandez MC, Nuñez ML, Miro E, Oliver A, Navarro F, Bou G. 2013. Characterization of the new AmpC  $\beta$ -lactamase FOX-8 reveals a single mutation, Phe313Leu, located in the R2 loop that affects ceftazidime hydrolysis. *Antimicrob Agents Chemother* 57:5158–5161. <http://dx.doi.org/10.1128/AAC.00818-13>.
39. Lefurgy ST, de Jong RM, Cornish VW. 2007. Saturation mutagenesis of Asn152 reveals a substrate selectivity switch in P99 cephalosporinase. *Protein Sci* 16:2636–2646. <http://dx.doi.org/10.1110/ps.073092407>.
40. Drawz SM, Bonomo RA. 2010. Three decades of  $\beta$ -lactamase inhibitors. *Clin Microbiol Rev* 23:160–201. <http://dx.doi.org/10.1128/CMR.00037-09>.
41. Matagne A, Misselyn-Bauduin AM, Joris B, Erpicum T, Granier B, Frere JM. 1990. The diversity of the catalytic properties of class A  $\beta$ -lactamases. *Biochem J* 265:131–146. <http://dx.doi.org/10.1042/bj2650131>.